High-dose Ionizing Radiation Regulates Gene Expression Changes in the MCF7 Breast Cancer Cell Line

VALENTINA BRAVATÀ[1*], LUIGI MINAFRA[1*], GIORGIO RUSSO[1], GIUSI IRMA FORTE[1], FRANCESCO P. CAMMARATA[1], MARILENA RIPAMONTI[1], CARLO CASARINO[1], GIUSEPPA AUGELLO[2], FRANCESCA COSTANTINI[2], GIOVANNA BARBIERI[2], CRISTINA MESSA[1,4,5] and MARIA C. GILARDI[1,3,5]

[1]*Institute of Bioimaging and Molecular Physiology, National Research Council (IBFM-CNR) -LATO, Cefalù (PA), Italy;*
[2]*Institute of Biomedicine and Molecular Immunology "Alberto Monroy"- National Research Council (IBIM-CNR), Palermo, Italy;*
[3]*Nuclear Medicine, San Raffaele Scientific Institute, Milan, Italy;*
[4]*Nuclear Medicine Center, San Gerardo Hospital, Monza, Italy;*
[5]*Department of Health Sciences, Tecnomed Foundation, University of Milano-Bicocca, Milan, Italy*

Abstract. *Background: Intraoperative electron radiation therapy (IOERT) is a therapeutic technique which administers a single high dose of ionizing radiation immediately after surgical tumor removal. IOERT induces a strong stress response: both tumor and normal cells activating pro- and antiproliferative cell signaling pathways. Following treatment, several genes and factors are differently modulated, producing an imbalance in cell fate decision. However, the contribution of these genes and pathways in conferring different cell radiosensitivity and radioresistance needs to be further investigated, in particular after high-dose treatments. Despite the documented and great impact of IOERT in breast cancer care, and the trend for dose escalation, very limited data are available regarding gene-expression profiles and cell networks activated by IOERT or high-dose treatment. The aim of the study was to analyze the main pathways activated following high radiation doses in order to select for potential new biomarkers of radiosensitivity or radioresistance, as well as to identify therapeutic targets useful in cancer care. Materials and Methods: We performed gene-expression profiling of the MCF7 human breast carcinoma cell line after treatment with 9- and 23-Gy doses (conventionally used during IOERT boost and exclusive treatments, respectively) by cDNA microarrays. Real-Time Quantitative Reverse Transcription PCR (qRT-PCR), immunofluorescence and immunoblot experiments were performed to validate candidate IOERT biomarkers. We also conducted clonogenic tests and cellular senescence assays to monitor for radiation-induced effects. Results: The analyses highlighted a transcriptome dependent on the dose delivered and a number of specific key genes that may be proposed as new markers of radiosensitivity. Cell and molecular traits observed in MCF7 cells revealed a typical senescent phenotype associated with cell proliferation arrest after treatments with 9- and 23-Gy doses. Conclusion: In this study, we report genes and cellular networks activated following high-dose IOERT. The selected validated genes were used to design two descriptive models for each dose delivered. We believe that this study could contribute to the understanding over the complex mechanisms which regulate cell radiosensitivity and radioresistance in order to improve personalized radiotherapeutic treatment.*

[*]These Authors contributed equally to this study.

Correspondence to: Luigi Minafra, e-mail: luigi.minafra@ibfm.cnr.it; Valentina Bravatà, e-mail: valentina.bravata@ibfm.cnr.it

Key Words: Intraoperative electron radiation therapy, IOERT, ionizing radiation, IR, MCF7 breast cancer cells, microarray.

Intraoperative radiation therapy is a therapeutic technique which consists of administering a single high dose of ionizing radiation (IR) immediately after surgical removal of tumor to destroy the residual cancer cells that may be left in the tumor site. Indeed, this typically represents a site at high risk for recurrence. The rationale for the use of this segmental radiation therapy in place of whole-breast irradiation is based on the finding that approximately 85% of local relapses are confined to the same quadrant of the breast from which the primary tumor was excised (1-4). Interest in intraoperative radiation therapy for breast cancer (BC) has increased in the last few years thanks to the development of the partial breast irradiation strategy with the aim of avoiding tumor recurrence. Intraoperative electron

Table I. *Primer sequences used for Real-Time Quantitative Reverse Transcription PCR analyses of MCF7 cells treated with 9 Gy and 23 Gy.*

Gene symbol	Full name	Forward primer 5'>3'	Reverse primer 5'>3'	Template size (base pairs)
ADAMTS9	ADAM metallopeptidase with thrombospondin type 1 motif, 9	tcgctccactgttcactgtc	ctgttgagggctctctctgg	297
ADRB1	Adrenoceptor beta 1	ctccttcttctgcgagctgt	agcacttggggtcgttgtag	266
ADRB2	Adrenoceptor beta 2	ctgctatgccaatgagacctg	gtcttgagggctttgtgctc	272
C2CD2	C2 calcium-dependent domain containing 2	ggccgttaatatccagcccaa	aagacgtggatgttcctcacc	252
CACNB2	Calcium channel, voltage-dependent, beta 2 subunit	tcctatggttcggcagactc	ttaccaatcgccctatccacc	286
Cav1	Caveolin 1, caveolae protein, 22kDa	tctctacaccgttcccatcc	tccaaatgccgtcaaaactgtg	219
CDC25C	Cell division cycle 25C	tctggccaaggaaagctcag	cgacagtaaggcagccact	207
CDC42	Cell division cycle 42	cttctttgctgctgcttcctg	ctgagcatcaggcaactcaag	224
CDKN1A/p21	Cyclin-dependent kinase inhibitor 1	cggcttcatgccagctactt	tcaccctgcccaaccttaga	245
FAM49B	Family with sequence similarity 49, member B	gggacttcccaggagaaaag	cagaagggtctgatggaagc	243
FAS	FAS cell surface death receptor	tcagtacggagttggggaag	caggccttccaagttctgag	207
Fos	FBJ murine osteosarcoma viral oncogene homolog	caacttcattcccacggtcac	tcccttcggattctccttttct	259
FosB	FBJ murine osteosarcoma viral oncogene homolog B	aacccaccctcatctcttcc	acccttcgcttctcctcttc	265
H2AFX	H2A histone family, member X	cgggcgtctgttctagtgttt	agtgattcgcgtcttcttgttg	293
HIST1H4E	Histone cluster 1, H4e	acatccagggcattaccaagc	agagtgcgtccctgtctctt	216
HIST2H2AB	Histone cluster 2, H2ab	gagtacctgaccgcggaaatt	aaagagcctttggggtgaatga	268
HIST2H2AC	Histone cluster 2, H2ac	tgtctggtcgtggcaaacaag	ctgttcagttcctcgtcgttg	286
HISTH1B	Histone cluster 1, H1b	gcattaagctgggcctcaaga	gctcttcgccacctttttgac	273
HISTH4B	Histone cluster 1, H4b	gataacatccaaggcatcacca	gaggccattggaagaaaactga	266
ITPR1	Inositol 1,4,5-trisphosphate receptor, type 1	gatcctggaggcagtaacca	ggacatcctctcccgaattga	226
JUN	JUN proto-oncogene	ccacgcaagagaagaaggac	gaaaagtcgcggtcactcact	280
JUNB	JUN B proto-oncogene	cggcagctacttttctggtc	cacgtggttcatcttgtgcag	261
LEF-1	Lymphoid enhancer-binding factor 1	agcagactggtttgcagtgaat	gatgacagttttgggcaaaggc	211
LMNB1	Lamin B1	ccttcttcccgtgtgacagt	cctcccattggttgatcctg	224
MMP9	Matrix metallopeptidase 9	gagaccggtgagctggata	tacacgcgagtgaaggtgag	236
MOAP1	Modulator of apoptosis 1	cgcctgtggtctggcatattt	cctcctgaacatccttccaag	222
NFKB	Nuclear factor of kappa light polypeptide gene enhancer in B-cells inhibitor, alpha	cagctggatgtgtgactgga	gtgggggaaaaatctccaaa	136
NR3C1	Nuclear receptor subfamily 3, group C, member 1 (glucocorticoid receptor)	actggctgtcgcttctcaatc	tgctgaactcttggggttctc	289
NR4A3	Nuclear receptor subfamily 4, group A, member 3	tccgctcctcctacactctc	tccatggtcagcttggtgtag	200
PLK1	Polo-like kinase 1	tgccacctcagtgacatgct	cagtgccgtcacgctctatg	265
SNAI1	SNAIL family zinc finger 1	gcgagctgcaggactctaat	ggacagagtcccagatgagc	135
TGFB2	Transforming growth factor, beta 2	gaccccacatctcctgctaa	taagctcaggaccctgctgt	268
TNF	Tumor necrosis factor	ctatctgggaggggtcttc	ggttgagggtgtctgaagga	201

radiation therapy (IOERT), using an electron linear accelerator, according to specific eligibility criteria may be: *exclusive* with the provision of a single radiation dose of 21-23 Gy corresponding to the administration of the entire sequence of a conventional adjuvant radiotherapy (RT), or an anticipated boost of 9-12 Gy, followed by conventional external RT to guarantee for optimal accuracy in dose delivery (5, 6).

Although preliminary results of partial breast irradiation with IOERT, either as an anticipated boost or as exclusive treatment, seem be promising in terms of local disease control, little information has been collected about the biological basis of the effects of IOERT, in particular those regarding molecular stress mechanisms (3, 4). To date, several radiobiology research groups have focused their studies on understanding the molecular mechanisms that confer radiosensitivity or radioresistance on cancer cells in order to improve RT effects. Both X-rays, mainly used in conventional external beam RT, and high-energy electrons generated by linear accelerators induce a strong cellular stress response, which leads to an imbalance in survival *versus* cell death decisions (7, 8). Increasing evidence is revealing that induction of cell death is a very complex mechanism accounting for the different therapeutic effects of IR (9, 10). Indeed, cell fate in response to IR is controlled by multiple signals that determine whether pro- or antiproliferative factors that normally function in equilibrium will ultimately predominate in response to the stress. Different IR-induced genes activate complex linked intracellular networks regulating several processes, such as cell-cycle progression, cell survival and death, DNA repair and inflammation (11-13). However, the contribution of these genes and the signaling

Table II. *PubMatrix analysis of selected validated genes. This table shows the number of manuscripts on selected genes and queries available on Pubmed tool.*

Gene symbol	Ionizing radiation	Radiation	Cancer	Breast cancer	Apoptosis	Inflammation	DNA damage	DNA repair
ADAMTS9	0	1	21	1	5	4	0	2
ADRB1	2	20	133	7	90	62	6	1
ADRB2	9	50	348	23	110	222	12	4
C2CD2	0	0	0	0	0	0	0	0
CACNB2	0	1	4	1	2	2	0	0
CAV1	9	34	503	100	115	65	8	6
CDC25C	60	92	612	75	367	12	255	52
CDC42	19	49	1330	171	359	125	28	9
CDKN1A/p21	5	5	20	3	23	1	13	3
FAM49B	0	0	0	0	0	2	0	0
FAS	376	823	7401	624	15646	1731	1272	168
FOS	280	937	4327	445	1356	977	406	193
FOSB	4	19	129	16	46	19	10	9
H2AFX	469	716	953	123	447	19	1300	786
HIST1H4E	0	0	0	0	0	0	0	0
HIST2H2AB	0	0	0	0	0	0	0	0
HIST2H2AC	0	0	0	0	0	0	0	0
HISTH1B	0	0	0	0	0	0	0	0
HISTH4B	0	0	0	0	0	0	0	0
ITPR1	6	11	68	2	49	5	2	0
JUN	11307	56905	263705	25505	29543	41202	9837	6466
JUNB	19	46	454	28	162	81	19	12
LEF-1	8	34	596	70	145	35	18	17
LMNB1	0	4	12	1	3	0	3	2
MMP9	22	78	1297	204	394	502	32	17
MOAP1	0	0	8	2	19	2	2	1
NFKB	15	41	258	39	186	189	34	17
NR3C1	0	4	54	5	21	22	3	5
NR4A3	0	2	87	5	42	24	4	7
PLK1	25	57	693	64	254	12	149	52
SNAI1	1	5	149	43	14	4	1	1
TGFB2	13	37	448	66	185	182	14	14
TNF	767	1993	19816	1407	16881	31724	1556	258

pathways involved in cellular response to high radiation doses is not entirely known. Despite the great interest of the scientific community regarding the clinical application of IR to various cancer types, a limited number of studies describe the molecular basis of IOERT effects. In particular, gene-expression profiles of BC cells treated with high IR doses, such as those delivered during IOERT, need to be explored (14, 15). It should be considered that BC is a heterogeneous and complex disease at both the molecular and clinical level (16-19), where often the failure of RT due to cell radioresistance may occur. The aim of this study was to analyze the main pathways activated following RT with high dose in order to select potential new biomarkers of radiosensitivity and radioresistance, as well as to identify therapeutic targets useful in BC care.

Herein we report the cell and gene expression response of human breast carcinoma MCF7 cells following IOERT treatment with 9 and 23 Gy doses.

Materials and Methods

IOERT. The NOVAC7 (Sortina IOERT Technologies, Vicenza, Italy) IOERT system producing electron beams of 4, 6, 8 and 10 MeV nominal energies was used to perform treatments at different tissue depths. The beam collimation was performed through a set of polymethylmethacrylate applicators: cylindrical tubes with a diameter ranging from 3 to 10 cm and face angle of 0˚-45˚. The electron accelerator system was calibrated under reference conditions defined by the International Atomic Energy Agency Technical Reports Series No. 398 "Adsorbed Dose Determination in External Beam Radiotherapy" (20). The irradiation setup and the dose distribution were studied by modeling electron and photon propagation with Monte Carlo methods, a flexible yet rigorous approach to simulate electron and photon transport. The simulations were performed with the GEANT4 toolkit (European Organization for Nuclear Research-CERN, Meyrin, Switzerland) widely adopted by the Medical Physics community to support technical and clinical issues in RT. For our purposes, we used the IOERT therapy application to simulate the

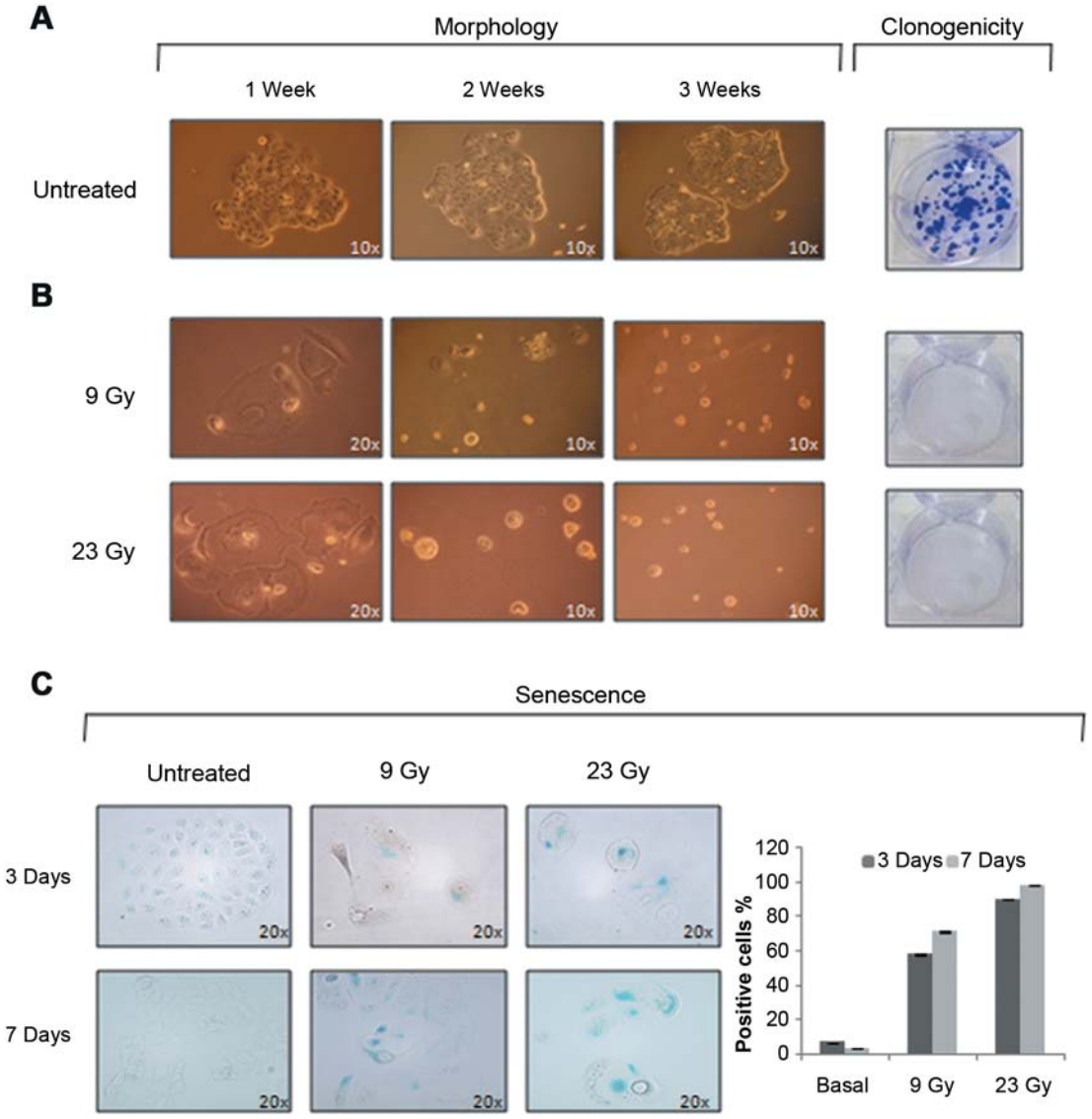

Figure 1. *A: Micrographs of MCF7 cell line after 1, 2, 3 weeks post Intraoperative electron radiation therapy (IOERT) for morphological evaluation and clonogenic survival assay (Untreated cells). B: MCF7 cells treated with 9 Gy and 23 Gy. C: Cell morphology and senescence-associated β-galactosidase (SA-β-Gal) activity in MCF7 cells treated with 9 Gy and 23 Gy, 3 and 7 days post IOERT. The graph displays the percentages of SA-β-Gal-positive cells (Basal = untreated cells).*

beam collimation system of the NOVAC7 from the electron exit window into air, passing through the applicator-collimator system, down to the cell plate (21). Cell irradiations were conducted with two dose values, 9 Gy to evaluate the IOERT treatment in the boost scheme and 23 Gy to study the *exclusive* modality to the 100% isodose and at a dose rate of 3.2 cGy/pulse.

Cell culture and clonogenic survival assay. The MCF7 human epithelial breast carcinoma cell line was purchased from the American Type Culture Collection (Manassas, VA, USA) and cultured in Dulbecco's Modified Eagle's medium supplemented with 10% Fetal bovine serum, and 1% penicillin/streptomycin in solution at 37˚C in an incubator with 5% CO_2. All cell culture media and supplements were obtained from Invitrogen (Carlsbad, CA, USA). Cells were seeded in 100-mm petri dishes or in 24-well plates 48 hours before treatments and were irradiated at subconfluence.

Clonogenic survival assay of MCF7 cells was performed according to the protocol published by Franken *et al*. (22). Briefly, 24 hours after irradiation, treated MCF7 cells were seeded in triplicate at a density of 200-1000 cells per well in a 6-well plate to assay the surviving fraction. Considering the high doses delivered, the clonogenic assay was also performed plating up to 10×10^4 cells in 100-mm Petri dishes. As control (basal), untreated cells were seeded in the same conditions in order to evaluate the plating efficiency.

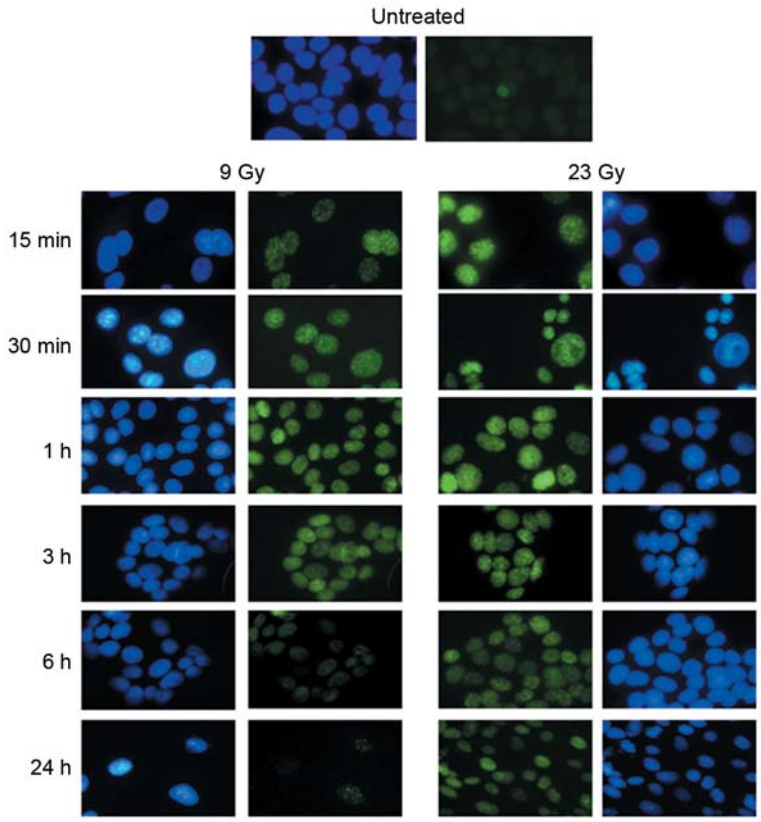

Figure 2. *Micrographs (×20) of gamma-H2AX immunofluorescence (γH2AX) analysis in MCF7 cells 15 and 30 min, and 1, 3, 6, and 24 h after exposure to 9 and 23 Gy. γH2AX foci: green; nuclei are counterstained with Hoechst in blue.*

Colonies were allowed to grow under normal cell culture conditions for two or three weeks and then were fixed and stained for 30 min with 6% glutaraldehyde and 0.5% crystal violet (both from Sigma-Aldrich, St. Louis, MO, USA). Colonies with more than 50 cells were counted manually under a Zeiss Axiovert phase-contrast microscope (Carl Zeiss, Göttingen, Germany). To evaluate the effect of cell radiation, cells throughout the course of the assays were monitored for cell morphology and growth pattern by photographing five random fields for each treatment under a phase-contrast microscope.

Senescence detection assay. Twenty-four hours after irradiation, MCF7 cells were seeded in triplicate at a density of 100 cells per well in two-well chamber slides. At three and seven days after irradiation, senescent cells were identified by a senescence-associated β-galactosidase (SA-β-gal) assay using a Senescence Cell Staining kit following the manufacturer's instructions (Sigma-Aldrich). Senescent cells were evaluated using a Zeiss Axioskop microscope (Carl Zeiss, Göttingen, Germany) under a ×20 lens. Five random fields of cells were photographed for each treatment and the percentage of SA-β-gal-positive cells was calculated.

Gamma-H2AX immunofluorescence analysis. Cells were grown on glass coverslips to reach 70% confluency before treatment. Control cells (basal, *i.e* untreated) were seeded in parallel. After defined times, cells on glass coverslips were fixed and permeabilized with cold methanol for 20 min, then washed in Phosphate buffered saline and stored at 4˚C until immunofluorescence analysis. PBS containing 2% bovine serum albumin and 0.1% Triton X-100 was used for blocking (blocking buffer) and antibody incubation. For γH2AX determination, Alexa Fluor® 488 Mouse anti-H2AX(p-S139) (BD Pharmingen™, San Diego, CA) antibody was diluted 1:200 in blocking buffer. Cell nuclei were counterstained with Hoechst 33342 (Life Technology, Carlsbad, CA). Gelvatol (Sigma-Aldrich, Saint Louis, MO, USA) was used as mounting medium. The images were captured by a Nikon Eclipse 80i (Chiyoda, Tokyo, Japan). γH2AX quantification was performed by ImageJ analysis software (http://rsb.info.nih.gov/ij/).

Whole-genome cDNA microarray expression analysis. Gene-expression profiling of MCF7 cells treated with 9 and 23 Gy IR doses was performed. Twenty-four hours after each treatment, MCF7 cells were harvested, counted and the pellet stored immediately at −80˚C. Total RNA was extracted from cells using Trizol and the RNeasy mini kit according to the manufacturer's guidelines (Invitrogen). RNA concentration and purity were determined spectrophotometrically using a Nanodrop ND-1000 (Thermo Scientific Open Biosystems, Lafayette, CO, USA) and RNA integrity, measured as RNA integrity number (RIN) values, was assessed using a Bioanalyzer 2100 (Agilent Technologies, Santa Clara, CA, USA). Only samples with a maximum RIN of 10 were

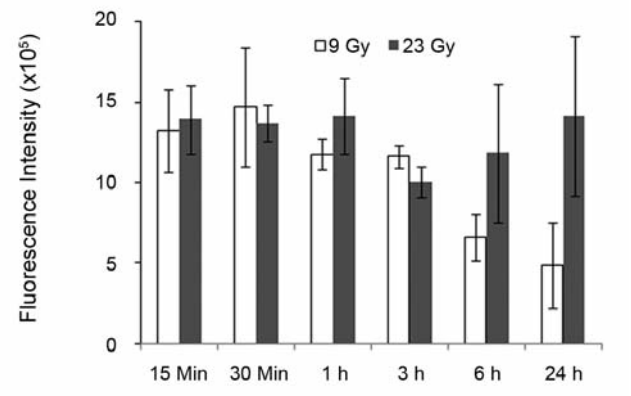

Figure 3. *Quantitative presentation of the mean gamma-H2AX fluorescence intensity for MCF7 cells 15 and 30 min, and 1, 3, 6, and 24 h after exposure to 9 and 23 Gy.*

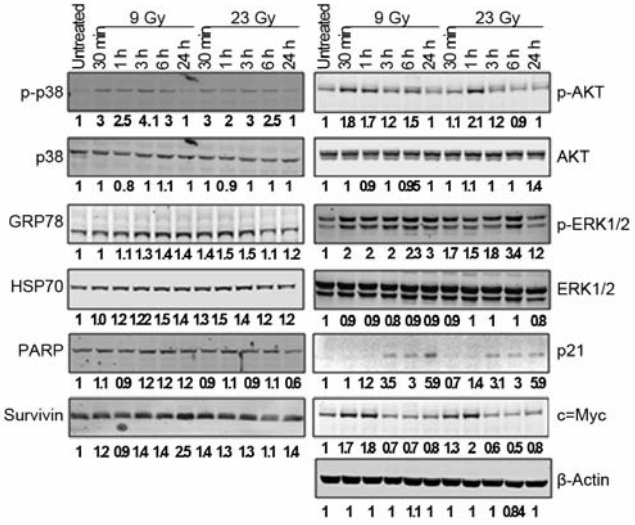

Figure 4. *Western blotting analysis for stress and survival response factors in MCF7 cells 15 and 30 min, and 1, 3, 6, and 24 h after exposure to 9 and 23 Gy.*

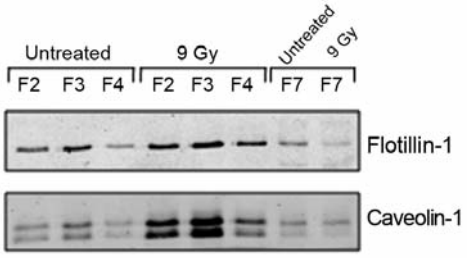

Figure 5. *Caveolin recruitment in lipid raft compartments of MCF7 cells treated with 9 Gy.*

used for further microarray analysis. Five hundred nanograms of total RNA were used for cRNA synthesis and labeling according to the Agilent Two-Color Microarray-Based Gene Expression Analysis protocol. Samples were labeled with Cy5 and Cy3 dye (Agilent Technologies). Fluorescent complementary cRNA samples (825 ng) were then hybridized onto Whole Human Genome 4×44K microarray (Agilent Technologies) GeneChips containing all known genes and transcripts of an entire human genome. Six replicates were performed. Array hybridization was conducted for 17 h at 65˚C. Images were made with an Agilent's DNA Microarray Scanner with Sure Scan high-Resolution Technology (Agilent Technologies) and analyzed using Feature Extraction expression software (Agilent Technologies) that found and placed microarray grids, rejected outlier pixels, accurately determined feature intensities and ratios, flagged outlier features, and calculated statistical confidences.

Statistical data analysis, background correction, normalization and summary of expression measures were conducted with GeneSpring GX 10.0.2 software (Agilent Technologies). Data were filtered using a two-step procedure: first the entities were filtered based on their flag values P (present) and M (marginal) and then filtered based on their signal intensity values, this enables very low signal values or those that have reached saturation to be removed. Statistically significant differences were computed by Student's *t*-test and the significance level was set at $p<0.05$. The false discovery rate (FDR) was used as a multiple test correction method. Average gene expression values of experimental groups were compared (on log scale) by means of a modified ANOVA ($p<0.05$). Genes were identified as being differentially expressed if they showed a fold-change (FC) of at least 1.5 with a *p*-value <0.05 compared to untreated MCF7 cells used as reference sample.

The data discussed in this publication have been deposited in the National Center for Biotechnology Information Gene Expression Omnibus (23) and are accessible through GEO Series accession number (http://www.ncbi.nlm.nih.gov/geo/query/acc.cgi?token=qnstoiigtlkbvkt&acc=GSE63667). Microarray data are available in compliance with Minimum Information About a Microarray Experiment standards.

MetaCore network analyses. The gene-expression profile of MCF7 cells irradiated with 9 Gy and 23 Gy were also analyzed by pathway analysis using the network building tool MetaCore GeneGo (Thomson Reuters, Philadelphia, PA, USA) consisting of millions of relationships between proteins derived from publications on proteins and small molecules (including direct protein interaction, transcriptional regulation, binding, enzyme-substrates, and other structural or functional relationships). Results, *i.e.* maps of protein lists from the uploaded dataset, were then compared with all the possible pathway maps for all the proteins in the database, and the *p*-value was calculated based on the hypergeometric distribution probability test. The most representative significantly changed networks were selected and analyzed.

Real-Time Quantitative Reverse Transcription PCR. Candidate genes for qRT-PCR analysis were chosen based on the microarray results. One microgram of total RNA was reverse-transcribed into cDNA with SuperScriptII reverse transcriptase according to the manufacturer's specifications (Invitrogen). One microliter of cDNA (50 ng RNA equivalent) was analyzed by real-time PCR (1 cycle 95˚C for 20 s and 40 cycles of 95˚C for 3 s and 60˚C for 30 s) in triplicate using a Fast 7500 Real-Time PCR System (Applied Biosystems, Carlsbad, CA). Amplification reactions were performed

Table III. *Up- and down-regulated genes in MCF7 cells treated with 9 Gy.*

Gene symbol	Gene ID	Description	Fold change	
			Microarray	qRT-PCR
ADAMTS9	56999	ADAM metallopeptidase with thrombospondin type 1 motif, 9	–3.37	0.04
ADRB1	153	Adrenoceptor beta 1	3.63	7.3
ADRB2	154	Adrenoceptor beta 2	4.6	2.96
CAV1	857	Caveolin 1, caveolae protein, 22kDa	6.4	4.2
CDC25C	995	Cell division cycle 25C	1.84	1.2
FAM49B	51571	Family with sequence similarity 49, member B	–3.13	0.4
FOS	2353	FBJ murine osteosarcoma viral oncogene homolog	1.84	19
FOSB	2354	FBJ murine osteosarcoma viral oncogene homolog B	2.38	14
HIST1H4E	8367	Histone cluster 1, H4e	2.61	15.9
ITPR1	3708	Inositol 1,4,5-trisphosphate receptor, type 1	–3.62	0.29
JUN	3725	JUN proto-oncogene	1.86	3.8
JUNB	3726	JUN B proto-oncogene	2.68	13.9
LEF-1	51176	Lymphoid enhancer-binding factor 1	–3.11	0.19
LMNB1	4001	Lamin B1	–2.26	0.53
MMP9	4318	Matrix metallopeptidase 9	1.70	1.6
MOAP1	64112	Modulator of apoptosis 1	–2.76	0.15
NR3C1	2908	Nuclear receptor subfamily 3, group C, member 1 (glucocorticoid receptor)	–2.28	0.3
NR4A3	8013	Nuclear receptor subfamily 4, group A, member 3	2.65	7.5
SNAI1	6615	SNAIL family zinc finger 1	1.72	3.6
TGFB2	7042	Transforming growth factor, beta 2	12.26	1.5
TNF	7124	Tumor necrosis factor	4.39	5.3
NFKB	4792	Nuclear factor of kappa light polypeptide gene enhancer in B-cells inhibitor, alpha	1.87	1.5

in a 20 μl reaction volume containing 10 pmoles of each primer and the Fast SYBR Green Master Mix according to the manufacturer's specifications (Applied Biosystems). Reaction specificity was controlled by post-amplification melting-curve analysis. The oligonucleotide primers were selected with Primer3 software [24-25] and tested for their human specificity using the NCBI database. Primer sequences (forward and reverse) used are listed in Table I. Quantitative data, normalized *versus* the rRNA for 18S gene, were analyzed by the average of triplicate cycle threshold (Ct) according to the $2^{-\Delta\Delta ct}$ method using SDS software (Applied Biosystems). The data shown were generated from three independent experiments and the values are expressed as the mean±SD relative to mRNA levels in the untreated MCF7 cells used as the control sample.

Isolation of raft fractions. To isolate the raft fractions (26), the treated and untreated cells were lysed in MBS buffer (25 mM 2-(N-morpholino)ethanesulfonic acid and 150 mM NaCl) containing 1% Triton X 100, anti-protease (4 μg/ml phenylmethanesulfonylfluoride, 3 μg/ml aprotinin, 1 μg/ml leupeptin) and the anti-phosphatase cocktails (1 mM Na_3VO_4 and 50 mM NaF) for 30 min on ice. The lysates mixed with an equal volume of 85% sucrose (w/v) in MBS buffer were placed at the bottom of a polycarbonate ultracentrifuge tube (Beckman Instruments, Palo Alto, CA, USA), then overlaid with 2 ml of 35% sucrose and 1 ml of 5% sucrose in MBS buffer containing 2 mM EDTA (pH 8), and the anti-protease and the anti-phosphatase cocktails, and were centrifuged at 100,000×g for 20 hours at 4˚C in a SW55Ti rotor (Beckman Instruments). Nine fractions of 550 μl each were collected from the top of the discontinuous sucrose gradient. The fractions containing the raft fractions were recovered from the 35%-5% interface (F2, F3 and F4). Therefore, 28 μl of fractions from 1 to 4 and 14 μl of fraction 7 were resolved by sodium dodecyl sulfate-polyacrylamide gel electrophoresis and absorbed on a nitrocellulose membrane (Hybond ECL; GE Healthcare Biosciences, Little Chalfont, Buckinghamshire,UK).

Western blot analysis. Whole cell lysates from 4 to 6×10^6 treated and untreated cells were obtained using RTB buffer (8 M urea, 2 M thiourea, 4% 3-[(3-cholamidopropyl)dimethylammonio]-1-propanesulfonate) supplemented with protease and phosphatase inhibitors (SIGMA-Aldrich) and western blots were performed using the methodology for the Odyssey® infrared imaging system (LI-COR Biosciences, Lincoln, Nebraska USA). After transfer, the nitrocellulose membranes were placed into Odyssey® blocking buffer (OBB; LI-COR) diluted in Tris-buffered saline and incubated for 1 h at room temperature. The following primary antibodies were used: Survivin (Abcam Limited, Cambridge, UK), β-actin (SIGMA, St. Louis, MO, USA), RAC-alpha serine/threonine-protein kinase (AKT), phospho-AKT, extracellular-signal-regulated kinases (ERK1/2), phospho-ERK1/2, phospho-p38, p38, poly (ADP-ribose) polymerase 1 (PARP) (Cell Signaling Technologies, Danvers, MA, USA), HSP70 (Santa Cruz, Biotechnology Inc., Heidelberg, Germany), caveolin-1, flotillin-1 (BD Transduction Laboratories, San Diego, CA), and 78 kDa glucose-regulated protein (GRP78) (SIGMA-Aldrich St. Louis, MO, USA). Primary and secondary antibodies conjugated to IRDye 800CW (LI-COR) or Alexa Fluor 680 (Molecular Probes, Invitrogen, Carlsbad, CA, USA) were appropriately diluted in OBB according to the manufacturer's specifications . Membranes were scanned on an Odyssey IR scanner (LI-COR Biotechnology, Lincoln, Nebraska USA) and images analyzed using the Odyssey imaging software

Table IV. *Up- and down- regulated genes in MCF7 cells treated with 23 Gy.*

Gene symbol	Gene ID	Description	Fold change	
			Microarray	qRT-PCR
ADAMTS9	56999	ADAM metallopeptidase with thrombospondin type 1 motif, 9	1.80	5.12
C2CD2	25966	C2 calcium-dependent domain containing 2	2.15	2.82
CACNB2	783	Calcium channel, voltage-dependent, beta 2 subunit	2.33	22
CDC42	998	Cell division cycle 42	−1.58	0.74
CDKN1A/p21	1026	Cyclin-dependent kinase inhibitor 1	1.6	2.67
FAM49B	51571	Family with sequence similarity 49, member B	2.24	1.5
FAS	355	FAS cell surface death receptor	2.42	2
H2AFX	3014	H2A histone family, member X	−1.51	0.78
HIST1H4E	8367	Histone cluster 1, H4e	−2.04	0.19
HIST2H2AB	317772	Histone cluster 2, H2ab	−3.01	0.63
HIST2H2AC	8338	Histone cluster 2, H2ac	−2.31	0.67
HISTH1B	3009	Histone cluster 1, H1b	−3.52	0.25
HISTH4B	8366	Histone cluster 1, H4b	−4.52	0.62
MOAP1	64112	Modulator of apoptosis 1	2.40	2.2
NR3C1	2908	Nuclear receptor subfamily 3, group C, member 1 (glucocorticoid receptor)	2.19	2.8
NR4A3	8013	Nuclear receptor subfamily 4, group A, member 3	2.24	4.1
PLK1	5347	Polo-like kinase 1	−1.55	0.23

3.0. Antibody signals were analyzed as integrated intensities of regions defined around the bands of interest in both channels.

Results

Clonogenicity, morphology and senescence analyses. In order to evaluate MCF7 cell viability in terms of reproductive capacity, we performed a clonogenic survival assay according to the method described by Franken *et al*. (22). Twenty-four hours after 9 and 23 Gy RT, cells were seeded, maintained under normal culture conditions and observed from two to three weeks later for the formation of colonies. The results showed that 9- and 23-Gy exposure inhibited the growth and proliferation of MCF7 cells, as their colony-forming ability was markedly impaired by IR and no colonies were observed following either treatment (Figure 1A and B).

To analyze high-dose radiation effects on cell morphology, cells throughout the course of the clonogenic assays were monitored by photographing random fields for each treatment under phase-contrast microscopy. MCF7 cell response in terms of morphology, observed after irradiation with 9 Gy and 23 Gy, was similar. As shown in Figure 1A and B, irradiated MCF7 cells displayed a large and flat cell shape, with evident macroscopic plasma membrane and nuclear alterations. These radiation-induced changes become visible starting from 72 h post treatment and increased within one week. The total detachment of cells from the culture substrate was observed progressively after two to three weeks. The cell traits observed suggest a typical senescent phenotype, the so-called 'fried egg', which is generally sustained by SA-β-Gal activity (27, 28).

To confirm the effect of IR on senescence induction, SA-β-Gal activity was examined after three and seven days of treatment. The number of cells exhibiting senescence-specific morphologies progressively increased in a dose- and time-dependent manner (Figure 1C). As shown in the graph, the number of cells that displayed SA-β-Gal activity gradually increased up to seven days. Collectively, these results indicate that 9 and 23 Gy IR doses induced senescence phenotypes in MCF7 cells.

γH2AX immunofluorescence analysis. It is well-known that histone H2AX is rapidly phosphorylated at serine 139 (γ-H2AX) following exposure to IR, with a consequent focus formation as a sensitive early cell response to the presence of DNA double-strand breaks (DSBs). To determine the time course of the appearance of γ-H2AX foci upon RT of MCF7 cells, we carried out direct immunofluorescence analyses after 15 min, 0.5, 1, 3, 6 and 24 h of exposure to 9 and 23 Gy IR doses. Figure 2 and 3 show that the formation of γ-H2AX foci occurred rapidly within 15 min after irradiation at both 9 and 23 Gy.

The quantification of γ-H2AX spots revealed that at 9 Gy the foci numbers gradually reduced, in particular after a recovery time of 6 and 24 h, but at 23 Gy, they remained quite high, up to 24 h after irradiation (Figure 2 and 3). These results suggest that foci formation in MCF7 cells is rapid, with a dose-dependent increase following exposure to RT.

Overview of cDNA microarray gene expression. In this study, a Two-Color Microarray-Based Gene Expression Analysis was

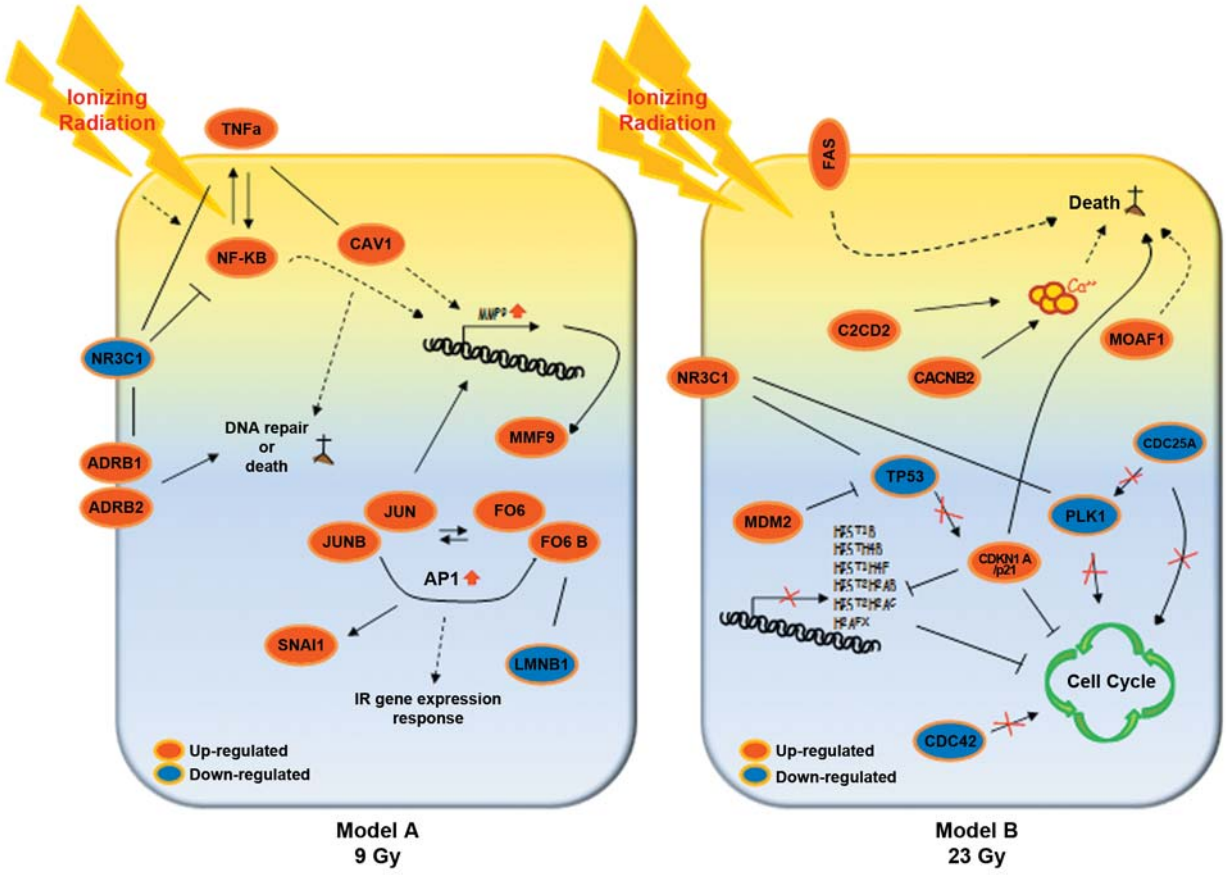

Figure 6. *Two descriptive models of genes and networks activated in MCF7 cells after treatment using the two doses of 9 Gy (A: model 1) and 23 Gy (B: model 2).*

conducted on MCF7 cells treated with 9 Gy, 23 Gy and on the untreated MCF7 cells, used as a reference sample. Comparative differential gene expression analysis revealed that 2,346 genes in MCF7 cells irradiated with 9 Gy had expression levels significantly altered by 1.5-fold or greater compared to the untreated reference group of MCF7 cells: 1,259 genes were down-regulated and 1087 were up-regulated. Moreover, comparative differential gene expression analysis revealed that 813 genes in MCF7 cells irradiated with 23 Gy had expression levels significantly altered by 1.5-fold or greater compared to the untreated MCF7 cells: 346 genes were down-regulated and 467 were up-regulated (Gene Expression Omnibus ID: GSE63667). Up- and down-regulated transcripts were selected and grouped according to their involvement in specific biological pathways using integrated pathway enrichment analysis with GeneGo MetaCore. Data sets were loaded into Metacore software and the top enriched canonical metabolic pathways were analyzed. The result of this mapping revealed the involvement of a set of factors controlling specific networks such as negative regulation of cellular processes, inflammation, tissue degradation, cell-cycle modulation, and chromatin modification in comparison with the reference sample. Candidate genes were selected, validated and analyzed using the PubMatrix tool (29) (Table II). This way, lists of terms such as gene names can be assigned to a genetic, biological, or clinical relevance in a flexible systematic fashion in order to test our assumptions.

Microarray validation experiments. Genes for validation were chosen based on two considerations: i) factors known to be modulated by IR; and ii) lesser-known genes involved in cell response to high radiation doses to be proposed as new molecular markers. In order to identify possible documented relationships between microarray gene expression lists and some processes known to be involved in cell response to IR treatment, we used the PubMatrix V2.1 tool. This way, bibliographic relationships between differentially expressed genes and some selected queries such as ionizing radiation, radiation, cancer, BC, apoptosis, inflammation, DNA damage and DNA repair were analyzed. Moreover, based on the microarray data set, PubMatrix results and MetaCore analyses, we chose 33 candidate genes, some of these were common to

MCF7 cells treated with 9 Gy and with 23 Gy, and performed qRT-PCR validation experiments (Table III and IV). In MCF7 cells treated with 9 Gy, 22 selected genes were validated. Fifteen genes known to be involved in positive regulation of gene expression, cell-cycle regulation and inflammation, namely: cell division cycle 25C (*CDC25C*), nuclear factor of kappa light polypeptide gene enhancer in B-cells (*NFKB*), transforming growth factor beta 2 (TGFB2), matrix metallopeptidase 9 (*MMP9*), adrenoceptor beta 2 (*ADRB2*), snail family zinc finger 1 (*SNAI1*), jun proto-oncogene (*JUN*), caveolin 1 (*CAV1*), tumor necrosis factor (*TNF*), adrenoceptor beta 1 (*ADRB1*), nuclear receptor subfamily 4, group A, member 3 (*NR4A3*), jun B proto-oncogene (*JUNB*), FBJ murine osteosarcoma viral oncogene homolog B (*FOSB*), histone cluster 1, H4e (*HIST1H4E*), FBJ murine osteosarcoma viral oncogene homolog (*FOS*), were found to be up-regulated. Seven genes involved in modulation of apoptosis and in cellular signaling processes, namely modulator of apoptosis 1 (*MOAP1*) and inositol 1,4,5-trisphosphate receptor, type 1 (*ITPR1*) and also ADAM metallopeptidase with thrombospondin type 1 motif 9 (*ADAMTS9*), lymphoid enhancer-binding factor-1 (*LEF-1*), nuclear receptor subfamily 3, group C, member 1 (*NR3C1*,) family with sequence similarity 49, member B (*FAM49B*) and lamin B1 (*LMNB1*) were down-regulated.

In MCF7 cells irradiated with 23 Gy, 17 selected genes were validated. Nine genes involved in cell death were up regulated, namely Fas cell surface death receptor (*FAS*), *MOAP1*, cyclin-dependent kinase inhibitor 1A (p21, Cip1) *CDKN1A, FAM49B, NR3C1, NR4A3, C2CD2, ADAMTS9* and calcium channel, voltage-dependent, beta 2 subunit (*CACNB2*), while eight genes of the histone cluster and involved in cell-cycle activation (polo-like kinase 1 (*PLK1*), histone cluster 1, H4e (*HIST1H4E*), *HISTH1B*, *HISTH4B, HIST2H2AB, HIST2H2AC, CDC42* and H2A histone family, member X (*H2AFX*)) were down regulated (Table III and IV).

Stress and survival response. Cell stress response was evidenced following both 9 Gy and 23 Gy IR treatments in time-course experiments and monitored by western blot analysis. In both cases, the expression of stress-activated phospho-p38 MAPK increased rapidly and then returned to the basal level after 24 h (Figure 4). In addition, a moderate increase in GRP78 and HSP70 expression occurred in time course post-irradiation. The activation of survival signals mediated by AKT and ERK1/2 kinases was also observed. In particular, our data showed an early activation of phospho-AKT with a maximum level at 30 min in cells irradiated with 9 Gy and at 1 hour in those irradiated with 23 Gy; the signal decreased over time and returned to basal levels after 24 h under both treatments. The phospho-ERK1/2 signal was activated at 30 min and remained activated all the time following both treatments (Figure 4). In addition, the morphological observation of treated cells showed no evidence of apoptosis induction. This was also confirmed at the molecular level. As shown in Figure 4, the apoptotic pathway did not seem to be activated during exposure to the two IR doses, as suggested by the absence of PARP fragmentation. The increase of expression of p21 protein, an inhibitor of cyclin-dependent kinases, and of survivin and the reduction of c-MYC expression, could have contributed to the block of cell proliferation observed in MCF7 cells after both IR treatments.

CAV1 determination. Based on the microarray dataset and on the documented but not yet understood role of CAV1 in BC and in cell response to IR, we studied CAV1 protein localization in cholesterol and glycosphingolipid-enriched membrane micro-domains, the lipid rafts, which are membrane domains where signaling complexes assemble (30). Therefore, after 24 h from 9 Gy treatment, MCF7 cells were lysed and the lipid raft compartments were isolated through a discontinuous sucrose gradient (31). The results of these experiments showed a significant recruitment of CAV1 (4.19-fold increase with respect to untreated MCF7 cells) to the low-density fractions (Figure 5, F2-F4) containing the lipid raft compartments. Flotillin-1 localization in the isolated fractions was also analyzed as a positive control of the raft compartments (Figure 5) (32). A lower increase of the amount of flotillin-1 (1.97-fold increase with respect to untreated MCF7 cells) in the raft fractions of treated cells was also observed, suggesting that the treatment of MCF7 cells could lead to a slight increase of the raft fraction compartments. Therefore, these results indicate that high IR dose treatment increases the lipid raft localization of CAV1.

Discussion

Despite the great interest of the scientific community regarding the clinical application of high-dose treatments, and in particular of IOERT on various cancer types, a limited number of studies describe its biological and molecular effects. In particular, gene-expression profiles of BC cells induced by high IR doses, such as those used during this type of RT, need to be further explored (14, 15).

The aim of the present study was to highlight cell and gene expression response following IOERT treatment with 9 and 23 Gy doses (IOERT *boost* and *exclusive*, respectively) to human breast adenocarcinoma MCF7 cell line. Although immortalized cell lines may present some limitations in predicting *in vivo* responses in humans, they remain well-established models in biomedicine for elucidating a complete understanding of cellular processes in cancer, including tumor response to radiation therapy.

Firstly, we evaluated cell viability in terms of reproductive capacity by performing a clonogenic survival assay and observed that 9- and 23-Gy doses inhibited growth and proliferation of MCF7 cells. The colony-forming ability was

markedly impaired by these high IR doses and no colonies were observed during two to three weeks after either treatment.

The exposure of cells to IR causes various types of damage, such as the creation of DNA DSBs. It is well known that histone H2AX is rapidly phosphorylated (γ-H2AX) following exposure to IR, forming discrete nuclear foci at sites of DSBs to trigger DNA repair mechanisms. Using immunofluorescence techniques, we evaluated the time-course for the appearance of γ-H2AX foci in MCF7 cells upon high-dose treatments and our data revealed that foci formation rapidly increased in a dose-dependent manner. If not adequately repaired, DSBs lead to cell clonogenicity loss *via* the generation of lethal chromosomal aberrations, the direct induction of apoptotic cell death or of cellular senescence (7, 10). Cellular senescence is an irreversible cell-cycle arrest, which limits the proliferative capacity of cells exposed to a sub-lethal dose of DNA-damaging agents, including IR, or oxidative stress. Recent data report that senescence may play a more significant role in the primary mechanism underlying the loss of the self-renewal capacity in IR- or drug-treated cancer cells (13, 27). The cell traits observed in MCF7 cells post high-dose treatment, such as the so-called 'fried egg', suggest a typical senescent phenotype, also confirmed by s SA-β-Gal activity (27, 28). Moreover, the number of cells exhibiting senescence-specific morphology gradually increased in a dose- and time-dependent manner. On the other hand, the morphological observation of treated cells showed no evidence of apoptosis induction and this was also confirmed at the molecular level. Western blot analysis revealed the absence of PARP fragmentation, suggesting that the apoptotic pathway did not seem to be activated. Some signals of stress and survival were induced early following treatments, such as p-p38 MAPK, GRP78, HSP70, p-AKT and p-ERK1/2 kinases. Furthermore, the senescence observed together with the increase of p21 and survivin protein expression and the reduction of c-MYC expression could contribute to cell proliferation arrest in MCF7 cells after both treatments.

In addition, 24 h after treatment, the intracellular network involved in cell response to high-dose treatment appeared to be dose-dependent. More precisely, our results show that the magnitude of transcriptional variation, defined as the number of differentially expressed genes, seemed to regulate cell fate decision in two different ways.

In order to highlight genes and networks activated after IR treatment, we used selected validated genes to design two descriptive models for each dose delivered (Figure 6A and B).

As reported in Figure 5A, the gene-expression profile of MCF7 cells irradiated at 9 Gy showed the involvement of key factors regulating gene transcription, cell cycle and inflammatory processes. Even if DNA represents the critical target of the biological effects of IR, the responses generated by high IR doses are not solely dedicated to safe-guarding genomic integrity, but also concern the activation of critical transcription factors such as NF-κB and activator protein 1 (AP1), both already found to be up-regulated following 9-Gy treatment (33, 34).

NFκB is a well-defined radiation-responsive transcription factor that regulates the gene expression of more than 200 target genes able to influence cell-cycle regulation after irradiation, to suppress apoptosis and to induce cellular transformation, proliferation, metastasis and inflammation in a wide variety of tumors (35). NF-κB is able to induce radioresistance by cell-cycle regulation, alterations in apoptosis and changes in the ability of cells to repair DNA damage; it has recently become an important target in the therapy of several chemoresistant/radioresistant types of cancer (36-38). IR persistently induces NF-κB DNA-binding activity and NF-κB-dependent TNFα transactivation and secretion, as described in both *in vitro* and *in vivo* studies (39, 40). Our results make this assumption because both NFKB and TNFA were up-regulated as shown in model 1 (Figure 6A). The exposure of mammalian cells to extracellular stress such as IR induces the expression of immediate early genes, such as *FOS* and *JUN*, and activates AP1 (41). AP1 is a heterodimeric transcription factor composed of FOS- and JUN-related proteins (42). As reported in Figure 6A, *JUN, JUNB, FOS* and *FOSB* were up-regulated after 9 Gy IR. Our data confirm previous studies indicating that *JUNB* gene is responsive to IR and is immediately induced after stimulation (43), revealing its important role in the early cell response process against radiation. AP1 proteins play an important role in the induction and development of late radiation effects in normal tissues. AP1 regulates the expression of several genes involved in oncogenic transformation and cellular proliferation such as those coding for MMPs, and TGFβ (42). MMPs are known to be up-regulated after radiation exposure and several recent studies have demonstrated an increase in MMP9 expression through NF-κB regulation, after RT, including after high radiation doses of 10 Gy (44-45). Moreover, in BC, MMP9 has been found up-regulated in M2 macrophages, able to promote tumor invasion and metastasis; macrophage inhibition following RT mightreduce tumor cell invasion (46). In addition, considering that AP1 activates the epithelial–mesenchymal transition marker *SNAI1*, overexpressed in MCF7 cells treated with 9 Gy and also in a variety of human malignancies such as BC, we speculated an EMT involvement in cell response to high IR doses (18, 19, 47). However, qRT-PCR assays for other EMT markers, such as those described recently by our group (18, 19), did not support this hypothesis (data not shown).

In order to study other lesser-known genes involved in cell response to high radiation doses for proposal as new molecular markers, we evaluated *ADRB1, ADRB2, LMNB1* and *NR3C1*, deregulated after IR with 9 Gy. *ADRB1* and *ADRB2* genes, up-regulated in MCF7 cells treated with 9 Gy, belong to a prototypic family of regulatory protein-coupled receptors that mediate the physiological effects of the hormone epinephrine

and the neurotransmitter norepinephrine (48). ADRB proteins are widely expressed in immune cells and play a role in modulating macrophagic function and mediating the apoptosis process after post-infarction heart failure. In particular, *ADRB2* was proposed as a novel UV radiation response gene but its role, which probably involves the activation of MDM2 and subsequent degradation of the tumor-suppressor protein p53, is far from being fully elucidated (48, 49).

As recently reported by Freund *et al*., LMNB1 is lost from primary human and murine cells when they are induced to senesce by DNA damage, replicative exhaustion, or oncogene expression. Moreover, *LMNB1* protein and mRNA decline in mouse tissue after senescence was induced by irradiation (50). Considering the senescence-specific phenotype we observed, a similar scenario, that for the first time to our knowledge, could also be proposed for MCF7 cells treated with 9 Gy of IR. Moreover, in both the proposed models, NR3C1 was deregulated but in opposite ways: under- and overexpressed in MCF7 cells treated with 9 Gy and 23 Gy, respectively (Figure 6A and B). This gene encodes for a glucocorticoid receptor involved in inflammatory responses, cellular proliferation, and chromatin-remodeling processes but limited information is available regarding its role in BC and after IR treatment. Moreover, this gene was associated with poor prognosis in estrogen receptor-negative BC and was also included in a five-gene expression signature indicative of the early-stage erb-b2 receptor tyrosine kinase-2 targeted therapy response (51-53). Thus, we hypothesize an interesting role for NR3C1 in MCF7 cells exposed to a high dose of IR, however, this needs further clarification.

The last gene described and up-regulated in model 1 is *CAV1* (Figure 5). This gene codes for an essential constituent protein of specialized plasma membrane invaginations called caveolae. It was recently described as a tumor suppressor, a prognostic marker of induction of metastasis in BC, as well as an essential modulator of cancer cell radiation and drug response (54-56). In addition, recent data have shown its role in radio- and chemoresistance of tumor cells (55). During the past decade, it has became evident that CAV1 plays a key role in cancer progression and metastasis, especially in BC. Hayashi and colleagues described a *CAV1* mutation at codon 132 (P132L) found in 16% of cases analyzed. The mutation-positive cases were mostly invasive scirrhous carcinomas associated with malignant BC progression (56). *CAV1* was described as a regulator of certain signaling proteins that are localized in lipid raft compartments. Interestingly, membrane re-organization in large domains of lipid rafts has been reported as being able to drive radiation-induced signal transmission in human carcinoma cells, underlying the impact of lipid rafts in cell response to IR (57-58).

Figure 6B shows descriptive model 2 of selected and validated genes proposed for responses of MFC7 cells treated with 23 Gy of IR. As is well-known, in addition to DNA damage and inhibition of DNA synthesis, IR induces down-regulation of histone mRNA levels in mammalian cells, through the G_1 checkpoint pathway (59). IR-induced inhibition of histone gene transcription depends on the p21 protein, which was found to up regulated in MCF7 cells treated with 23 Gy. It has been reported that exposure to high and low linear energy transfer radiation negatively regulates histone gene expression in human lymphoblastoid and colon cancer cell lines regardless of p53 status (60). In our model, the p53 gene was down-regulated after 23 Gy treatment, while its negative regulator *MDM2* was up-regulated, thus it did not seem to be active in regulating histone production or in exerting a crucial role at 24 h post-treatment. In line with these data, in the gene-expression profile of MCF7 cells treated with 23 Gy, a large number of histone genes were down-regulated. Six of them were validated, confirming their massive down-regulation after a high dose of IR; to our knowledge, this is the first time this has been described in BC cells (Table IV) (61).

In addition, as proposed by Du *et al*., intracellular calcium levels could play an important role in regulating IR-induced cell-cycle arrest, possibly mediating chromatin structure (62). In line with these assumptions, as shown in model 2, the following two calcium-related genes, *CACNB2* and *C2CD2* were up-regulated, suggesting an increase of the calcium level after IR (Figure 6B). Cytosolic Ca^{2+} increase was reportedly involved in regulating apoptosis induced by UV or TNFα (63), but very limited information is available regarding CACNB2 and C2CD2 function. In our model, these two proteins might function as modulators of cell death that has not yet been described, even if their role after a high dose of IR needs to be further investigated. In addition, *MOAP1* and *FAS* were up-regulated (Table IV and Figure 6B). The up-regulation of *MOAP1* has been described not as a consequence of apoptosis but as an early event in the apoptotic signaling process, which has not yet been clarified. An increase of MOAP1 levels may sensitize cells to stimuli that promote cell death, but no data are currently available regarding its relation with IR (64). Moreover, *FAS* up-regulation after IR exposure has been described by several authors (65-69).

As described above, in MCF7 cells treated with 23 Gy, cell-cycle arrest may also be suggested by the down-regulation of its positive modulators such as *PLK1, CDC42* and *CDC25A*, which were down-regulated, and by the up-regulation of CDKN1A/p21. PLK1 is essential for mitosis because it promotes mitotic entry by phosphorylating cyclin B1 and CDK1, and initiates mitotic exit by activating the anaphase-promoting complex. Overexpression of PLK1 promotes chromosomal instability and aneuploidy by G_2-M DNA damage and spindle checkpoints (70). Recently, PLK1 targeting with small molecule inhibitors, in combination with RT, has been proposed as a novel strategy in cancer treatment, which requires further investigation (70).

CDC42 regulates the bipolar attachment of spindle microtubules to kinetochores before chromosome ingression

in metaphase (71). This protein is mainly involved in actin cytoskeleton organization but also in a huge number of other cellular processes, such as gene transcription, cell proliferation and survival.

CDC25 protein phosphatases are critical components of cell engines that function to drive cell-cycle transitions by dephosphorylating and activating CDKs (72). Overexpression of CDC25 family proteins has been reported in a variety of human cancer types, including BC (73-75). Few studies have been carried out to explore the different roles of CDC25 in mediating radioresistance through the activation of cell-cycle checkpoints, however, even the available data are still unclear (76).

In summary, gene profiles after high-dose exposure to RT, and specifically after IOERT, can vary extensively depending on the dose delivered. Both the high doses of IR used in our experiments altered several genes and processes, providing the opportunity to explore molecular target-directed interventions to enhance tumor response to RT.

Conclusion

The main goal of IOERT is to deprive cancer cells of their reproductive potential, forcing them to undergo cell death. Despite the great interest of the scientific community regarding high-dose clinical applications for various cancer types, only a limited number of studies describe the biological and molecular basis of high-dose effects, and specifically after IOERT (77). In order to highlight genes and cellular networks activated after high single-dose treatments, and to select potential new biomarkers of radiosensitivity and radioresistance, we used validated genes to design two descriptive models for each dose delivered. For MCF7 treated with 9 Gy and 23 Gy, we suggest dose-dependent gene-expression profiles that might regulate cell-fate decision in two different ways. The high-dose treatments inhibited the growth and proliferation of MCF7 cells and the post-irradiation cell traits showed a typical senescent phenotype, confirmed by senescence-SA-β-Gal activity which increased in a dose- and time-dependent manner. We described the involvement of known genes also related to the effects of lower doses of IR and introduced novel ones able to activate molecular networks that might contribute to guiding cell-fate decision. We trust that this study will contribute to the exploration of molecular target-directed interventions in order to improve personalized IR treatments for BC.

Conflicts of Interest

The Authors declare that they have no competing interests.

Acknowledgements

This work was supported by FIRB/MERIT project (RBNE089KHH). The Authors thank Marylia Di Stefano, Antonina Azzolina and Patrizia Rubino for their excellent technical assistance.

References

1 Bernier J, Viale G, Orecchia R, Ballardini B, Richetti A, Bronz L, Franzetti-Pellanda A, Intra M and Veronesi U: Partial irradiation of the breast: Old challenges, new solutions. Breast *15*: 466-75, 2006.

2 Offersen BV, Overgaard M, Kroman N and Overgaard J: Accelerated partial breast irradiation as part of breast conserving therapy of early breast carcinoma: a systematic review. Radiother Oncol *90*: 1-13, 2009.

3 Veronesi U, Orecchia R, Luini A, Galimberti V, Zurrida S, Intra M, Veronesi P, Arnone P, Leonardi MC, Ciocca M, Lazzari R, Caldarella P, Rotmensz N, Sangalli C, Sances D and Maisonneuve P: Intraoperative radiotherapy during breast conserving surgery: a study on 1,822 cases treated with electrons. Breast Cancer Res Treat *124*: 141-51, 2010.

4 Kraus-Tiefenbacher U, Bauer L, Scheda A, Schoeber C, Schaefer J, Steil V and Wenz F: Intraoperative radiotherapy (IOERT) is an option for patients with localized breast recurrences after previous external-beam radiotherapy. BMC Cancer *7*: 178, 2007.

5 Wallner P, Arthur D, Bartelink H Connolly J, Edmundson G, Giuliano A, Goldstein N, Hevezi J, Julian T, Kuske R, Lichter A, McCormick B, Orecchia R, Pierce L, Powell S, Solin L, Vicini F, Whelan T, Wong J and Coleman CN, Workshop Participants: Workshop on partial breast irradiation: state of the art and the science. J Natl Cancer Inst *96*: 175-184, 2004.

6 Smith BD, Arthur DW, Buchholz TA, Haffty BG, Hahn CA, Hardenbergh PH, Julian TB, Marks LB, Todor DA, Vicini FA, Whelan TJ, White J, Wo JY and Harris JR: Accelerated partial breast irradiation consensus statement from the American Society for Radiation Oncology (ASTRO). Int J Radiat Oncol Biol Phys *74*: 987-1001, 2009.

7 Lomax ME, Folkes LK and O'Neill P: Biological consequences of radiation-induced DNA damage: relevance to radiotherapy. Clin Oncol (R Coll Radiol) *25*: 578-85, 2013.

8 Multhoff G and Radons J: Radiation, inflammation, and immune responses in cancer. Front Oncol *2*: 58, 2012.

9 Eriksson D and Stigbrand T: Radiation-induced cell death mechanisms. Tumour Biol *31*: 363-72, 2010.

10 Surova O and Zhivotovsky B: Various modes of cell death induced by DNA damage. Oncogene *32*: 3789-97, 2013.

11 West CM and Barnett GC: Genetics and genomics of radiotherapy toxicity: towards prediction. Genome Med *3(8)*: 52, 2011.

12 Di Maggio FM, Minafra L, Forte GI, Cammarata FP, Lio D, Messa C, Gilardi MC and Bravatà V: Portrait of inflammatory response to ionizing radiation treatment. Journal of Inflammation *12:* 14, 2015.

13 Golden EB, Pellicciotta I, Demaria S, Barcellos-Hoff MH and Formenti SC: The convergence of radiation and immunogenic cell death signaling pathways. Front Oncol *2*: 88, 2012.

14 Xu QY, Gao Y, Liu Y, Yang WZ and Xu XY: Identification of differential gene expression profiles of radioresistant lung cancer cell line established by fractionated ionizing radiation *in vitro*. Chin Med J (Engl) *121*: 1830-7, 2008.

15 Snyder AR, Morgan WF: Gene expression profiling after irradiation: clues to understanding acute and persistent responses? Cancer Metastasis Rev *23*: 259-68, 2004

16 Bravatà V, Cammarata FP, Forte GI and Minafra L: "Omics" of HER2-positive breast cancer. OMICS *17*: 119-29, 2013.

17 Bravatà V, Stefano A, Cammarata FP, Minafra L, Russo G, Nicolosi S, Pulizzi S, Gelfi C, Gilardi MC and Messa C: Genotyping analysis and ^{18}F-FDG uptake in breast cancer patients: a preliminary research. J Exp Clin Cancer Res *32*: 23, 2013.
18 Minafra L, Norata R, Bravatà V, Viola M, Lupo C, Gelfi C and Messa C: Unmasking epithelial–mesenchymal transition in a breast cancer primary culture: a study report. BMC Res Notes *5*: 343, 2012.
19 Minafra L, Bravatà V, Forte GI, Cammarata FP, Gilardi MC and Messa C: Gene expression profiling of epithelial–mesenchymal transition in primary breast cancer cell culture. Anticancer Res *34*: 2173-83, 2014.
20 International Atomic Energy Agency: Adsorbed Dose Determination in External Beam Radiotherapy. An International Code of Practice for Dosimetry Based on Standards of Absorbed Dose to Water. Technical Reports Series No. 398, Vienna, 2000.
21 Russo G, Casarino C, Arnetta G, Candiano G, Stefano A, Alongi F, Borasi G, Messa C and Gilardi MC: Dose distribution changes with shielding disc misalignments and wrong orientations in breast IOERT: a Monte Carlo-GEANT4 and experimental study. J Appl Clin Med Phys *13*: 3817, 2012.
22 Franken NAP, Rodermond HM, Stap J, Haveman J and van Bree C: Clonogenic assay of cells *in vitro*. Nature Protocols *1*: 2315-2319, 2006.
23 Edgar R, Domrachev M and Lash AE: Gene Expression Omnibus: NCBI gene expression and hybridization array data repository. Nucleic Acids Res *30*: 207-210, 2002.
24 Rozen S and Skaletsky HJ: Primer3 on the WWW for general users and for biologist programmers. In: Bioinformatics Methods and Protocols: Methods in Molecular Biology. Krawetz S and Misener S (eds.). Humana Press, Totowa, NJ: 365-386, 2000.
25 Primer3 tool. http//fokker.wi.mit.edu/primer3.
26 Xavier R, Brennan T, Li Q, McCormack C and Seed B: Membrane compartmentation is required for efficient T cell activation. Immunity *8*: 723-732, 1998.
27 Panganiban RA, Snow AL and Day RM: Mechanisms of radiation toxicity in transformed and non-transformed cells. Int J Mol Sci *4*: 15931-58, 2013.
28 Jan M van Deursen: The role of senescent cells in ageing. Nature *509*: 439-446, 2014.
29 Becker KG, Hosack DA, Dennis G Jr, Lempicki RA, Bright TJ, Cheadle C and Engel J: PubMatrix: a tool for multiplex literature mining. BMC Bioinformatics *4*: 61,2003.
30 Lingwood D and Simons K: Lipid rafts as a membrane-organizing principle. Science *327*: 46-50, 2010.
31 Barbieri G1, Rimini E and Costa MA: Effects of human leukocyte antigen (HLA)-DR engagement on melanoma cells. Int J Oncol *38(6)*: 1589-95, 2011.
32 Stuermer CA, Lang DM, Kirsch F, Wiechers M, Deininger SO and Plattner H: Glycosylphosphatidyl inositol-anchored proteins and fyn kinase assemble in noncaveolar plasma membrane microdomains defined by reggie-1 and -2. Mol Biol Cell *12*: 3031-3045, 2001.
33 Dent P, Yacoub A, Fisher PB, Hagan MP and Grant S: MAPK pathways in radiation responses. Oncogene 22: 5885-96, 2003.
34 McBride WH, Iwamoto KS, Syljuasen R, Pervan M and Pajonk F: The role of the ubiquitin/proteasome system in cellular responses to radiation. Oncogene *22*: 5755-73, 2003.
35 Aravindan S, Natarajan M, Ramraj SK, Pandian V, Khan FH, Herman TS and Aravindan N: Abscopal effect of low-LET γ-radiation mediated through Rel protein signal transduction in a mouse model of non targeted radiation response. Cancer Gene Ther *21*: 54-9, 2014.
36 Chen X, Shen B, Xia L, Khaletzkiy A, Chu D, Wong JY and Li JJ: Activation of nuclear factor κB in radioresistance of TP53-inactive human keratinocytes. Cancer Res *62*: 1213-21, 2002.
37 Starenki D, Namba H, Saenko V, Ohtsuru A and Yamashita S: Inhibition of nuclear factor-kappaB cascade potentiates the effect of a combination treatment of anaplastic thyroid cancer cells. J Clin Endocrinol Metab *89*: 410-8, 2004.
38 Yamamoto Y and Gaynor RB: Therapeutic potential of inhibition of the NF-κB pathway in the treatment of inflammation and cancer. J Clin Invest *107*: 135-42, 2001.
39 Veeraraghavan J, Natarajan M, Aravindan S, Herman TS and Aravindan N: Radiation-triggered tumor necrosis factor (TNF)-α–NFκB cross-signaling favors survival advantage in human neuroblastoma cells. J Biol Chem *286*: 21588-600, 2011.
40 Aravindan S, Natarajan M, Awasthi V, Herman TS and Aravindan N: Novel synthetic monoketone transmute radiation-triggered NFκB-dependent TNFα cross-signaling feedback maintained NFκB and favors neuroblastoma regression. PLoS One *8(8)*: e72464, 2013.
41 Zhou H, Gao J, Lu ZY, Lu L, Dai W and Xu M: Role of c-Fos/JunD in protecting stress-induced cell death. Cell Prolif *40*: 431-44, 2007.
42 Benkoussa M, Brand C, Delmotte MH, Formstecher P and Lefebvre P: Retinoic acid receptors inhibit AP1 activation by regulating extracellular signal-regulated kinase and CBP recruitment to an AP1-responsive promoter. Mol Cell Biol *22*: 4522-34, 2002.
43 Kajanne R, Miettinen P, Tenhunen M, Leppä S: Transcription factor AP1 promotes growth and radioresistance in prostate cancer cells. Int J Oncol *35*: 1175-82, 2009.
44 Chiang PC, Chou RH, Chien HF, Tsai T and Chen CT: Chloride intracellular channel 4 involves in the reduced invasiveness of cancer cells treated by photodynamic therapy. Lasers Surg Med *45*: 38-47, 2013.
45 Speake WJ, Dean RA, Kumar A, Morris TM, Scholefield JH and Watson SA: Radiation induced MMP expression from rectal cancer is short lived but contributes to *in vitro* invasion. Eur J Surg Oncol *31*: 869-74, 2005.
46 Che J, Zhang FZ, Zhao CQ, Hu XD and Fan SJ: Cyclopamine is a novel Hedgehog signaling inhibitor with significant antiproliferative, anti-invasive and anti-estrogenic potency in human breast cancer cells. Oncol Lett *5(4)*: 1417–1421, 2013.
47 Sun M, Guo X, Qian X, Wang H, Yang C, Brinkman KL, Serrano-Gonzalez M, Jope RS, Zhou B, Engler DA, Zhan M, Wong ST, Fu L and Xu B.: Activation of the ATM-SNAIL pathway promotes breast cancer metastasis. J Mol Cell Biol *4*: 304-15, 2012.
48 Yang G, Zhang G Pittelkow MR, Ramoni M and Tsao H: Expression profiling of UVB response in melanocytes identifies a set of p53-target genes. J Invest Dermatol *126*: 2490-506, 2006.
49 Sood R, Ritov G, Richter-Levin G and Barki-Harrington L: Selective increase in the association of the β2 adrenergic receptor, β Arrestin-1 and p53 with Mdm2 in the ventral hippocampus one month after underwater trauma. Behav Brain Res *240*: 26-8, 2013.
50 Freund A, Laberge RM, Demaria M and Campisi J: Lamin B1 loss is a senescence-associated biomarker. Mol Biol Cell *23*: 2066-75, 2012.

51 Damaraju S, Murray D, Dufour J, Carandang D, Myrehaug S, Fallone G, Field C, Greiner R, Hanson J and Cass CE, Parliament M: Association of DNA repair and steroid metabolism gene polymorphisms with clinical late toxicity in patients treated with conformal radiotherapy for prostate cancer. Clin Cancer Res *12*: 2545-54, 2006.

52 Pan D, Kocherginsky M and Conzen SD: Activation of the glucocorticoid receptor is associated with poor prognosis in estrogen receptor-negative breast cancer. Cancer Res *71*: 6360-70, 2011.

53 O'Neill F, Madden SF, Aherne ST, Clynes M, Crown J, Doolan P and O'Connor R: Gene expression changes as markers of early lapatinib response in a panel of breast cancer cell lines. Mol Cancer *11*: 41, 2012.

54 Patani N, Martin LA, Reis-Filho JS and Dowsett M: The role of caveolin-1 in human breast cancer. Breast Cancer Res Treat *131*: 1-15, 2012.

55 Hehlgans S and Cordes N: Caveolin-1: an essential modulator of cancer cell radio-and chemoresistance. Am J Cancer Res *1*: 521-30, 2011.

56 Hayashi K, Matsuda S, Machida K, Yamamoto T, Fukuda Y, Nimura Y, Hayakawa T and Hamaguchi M: Invasion activating caveolin-1 mutation in human scirrhous breast cancers. Cancer Res *61*: 2361-4, 2001.

57 Bionda C, Hadchity E, Alphonse G, Chapet O, Rousson R, Rodriguez-Lafrasse C and Ardail D: Radioresistance of human carcinoma cells is correlated to a defect in raft membrane clustering. Free Radic Biol Med *43*: 681-6942007.

58 Rotolo J, Stancevic B, Zhang J, Hua G, Fuller J, Yin X, Haimovitz-Friedman A, Kim K, Qian M, Cardó-Vila M, Fuks Z, Pasqualini R, Arap W and Kolesnick R: Anti-ceramide antibody prevents the radiation gastrointestinal syndrome in mice. J Clin Invest *122*: 1786-1790, 2012.

59 Su C, Gao G, Schneider S, Helt C, Weiss C, O'Reilly MA, Bohmann D and Zhao J: DNA damage induces down regulation of histone gene expression through the G1 checkpoint pathway. EMBO J *23*: 1133-43, 2004.

60 Meador JA, Ghandhi SA and Amundson SA: p53-independent down-regulation of histone gene expression in human cell lines by high- and low-LET radiation. Radiat Res *175*: 689-99, 2011.

61 Bird AW, Yu DY, Pray-Grant MG, Qiu Q, Harmon KE, Megee PC, Grant PA, Smith MM and Christman MF: Acetylation of histone H4 by Esa1 is required for DNA double-strand break repair. Nature *419*: 411-5, 2002.

62 Du YC, Gu S, Zhou J, Wang T, Cai H, Macinnes MA, Bradbury EM and Chen X: The dynamic alterations of H2AX complex during DNA repair detected by a proteomic approach reveal the critical roles of Ca(2+)/calmodulin in the ionizing radiation-induced cell cycle arrest. Mol Cell Proteomics *5*: 1033-44, 2006.

63 Lao Y and Chang DC: Mobilization of Ca^{2+} from endoplasmic reticulum to mitochondria plays a positive role in the early stage of UV- or TNFα-induced apoptosis. Biochem Biophys Res Commun *373*: 42-7, 2008.

64 Fu NY, Sukumaran SK and Yu VC: Inhibition of ubiquitin-mediated degradation of MOAP1 by apoptotic stimuli promotes BAX function in mitochondria. Proc Natl Acad Sci USA *104*: 10051-6, 2007.

65 Kim MJ1, Lee KH and Lee SJ. Ionizing radiation utilizes c-JUN N-terminal kinase for amplification of mitochondrial apoptotic cell death in human cervical cancer cells. FEBS J *275*: 2096-108, 2008.

66 Sheard MA: Ionizing radiation as a response enhancing agent for CD95-mediated apoptosis. Int J Cancer *96*: 213-220, 2001.

67 Fulda S, Scaffidi C, Pietsch T, Krammer PH, Peter ME and Debatin KM: Activation of the CD95 (APO1⁄ FAS) pathway in drug- and gamma-irradiation induced apoptosis of brain tumor cells. Cell Death Differ *10*: 884-893, 1998.

68 Lin J, Yang Q, Wilder PT, Carrier F and Weber DJ: The calcium-binding protein S100B down-regulates p53 and apoptosis in malignant melanoma. J Biol Chem *285*: 27487-98, 2010.

69 Mao XW, Green LM, Mekonnen T, Lindsey N and Gridley DS: Gene expression analysis of oxidative stress and apoptosis in proton-irradiated rat retina. In Vivo *24*: 425-30, 2010.

70 Harris PS, Venkataraman S, Alimova I, Harris PS, Venkataraman S and Alimova I: Polo-like kinase 1 (PLK1) inhibition suppresses cell growth and enhances radiation sensitivity in medulloblastoma cells. BMC Cancer *12*: 80, 2012.

71 Yasuda S, Oceguera-Yanez F, Kato T, Yasuda S, Oceguera-Yanez F and Kato T: Cdc42 and mDia3 regulate microtubule attachment to kinetochores. Nature *428*: 767-71, 2004.

72 Lee G, Origanti S, White LS, Lee G, Origanti S and White LS: Contributions made by CDC25 phosphatases to proliferation of intestinal epithelial stem and progenitor cells. Plos One *6*: e15561, 2011.

73 Boutros R, Lobjois V and Ducommun B. CDC25 phosphatases in cancer cells: Key players? Good targets? Nat Rev Cancer *7*: 495-507, 2007.

74 Ray D and Kiyokawa H. CDC25A phosphatase: a rate-limiting oncogene that determines genomic stability. Cancer Res *68*: 1251-3, 2008.

75 Zhao Y, Cui Y, Han J, Zhao Y, Cui Y and Han J: Cell division cycle 25 homolog c effects on low-dose hyperradiosensitivity and induced radioresistance at elevated dosage in A549 cells. J Radiat Res *53*: 686-94, 2012.

76 Li J, Yang CX, Mei ZJ, Li J, Yang CX and Mei ZJ: Involvement of CDC25C in cell-cycle alteration of a radioresistant lung cancer cell line established with fractionated ionizing radiation. Asian Pac J Cancer Prev *14*: 5725-30, 2013.

77 Minafra L and Bravatà V: Cell and molecular response to IOERT treatment. Transl Cancer Res *3*: 32-47, 2014.

Received February 2, 2015
Revised February 17, 2015
Accepted February 20, 2015